

Acoustic and elastic numerical wave simulations by recursive spatial derivative operators

Dan Kosloff¹, Reynam C. Pestana², and Hillel Tal-Ezer³

ABSTRACT

A new scheme for the calculation of spatial derivatives has been developed. The technique is based on recursive derivative operators that are generated by an L_∞ fit in the spectral domain. The use of recursive operators enables us to extend acoustic and elastic wave simulations to shorter wavelengths. The method is applied to the numerical solution of the 2D acoustic wave equation and to the solution of the equations of 2D dynamic elasticity in an isotropic medium. An example of reverse-time migration of a synthetic data set shows that the numerical dispersion can be significantly reduced with respect to schemes that are based on finite differences. The method is tested for the solutions of the equations of dynamic elasticity by comparing numerical and analytic solutions to Lamb's problem.

INTRODUCTION

Numerical solution of acoustic and elastic equations is routinely used for generating synthetic seismic surveys. These simulations are also the basis of reverse-time migration. An effective numerical simulator must be both accurate and computationally efficient. The generation of effective numerical simulators has been the topic of active research in recent years.

The accuracy and efficiency of the numerical simulation depend on the method used for calculating the spatial derivatives in the wave equation and on the method for the time integration. For the time integration, second-order differencing in time is the simplest method; however, with this approach, numerical dispersion is always present unless extremely small time steps are used, which in turn make the numerical simulation very costly. Dablain (1986) presented a high-order time-integration scheme that reduces numerical dispersion

and, for a given accuracy, improves computational efficiency. Kosloff et al. (1989), Liu et al. (2009), and Stoffa and Pestana (2009) introduced more accurate and efficient time-integration schemes that allow an arbitrary time-step size; thus, the time-integration error can be made arbitrarily small without compromising numerical efficiency. The main source of errors in the numerical calculation is therefore in the approximation of spatial derivatives.

For the spatial derivative approximation, the fastest and least accurate method is second-order finite differences, whereas the pseudospectral method is the most accurate but considerably slower. In general, there is a trade-off: For a specified accuracy, a lower order method will require a larger number of grid points with a small number of calculations per point, whereas a higher order method will require fewer grid points but more calculations per point. Examination of the numerical phase velocity dispersion curves for explicit finite-difference schemes shows that although higher order schemes improve the accuracy, there is a saturation effect whereby the rate of improvement per order of the difference operator decreases for higher orders. Experience indicates that the most economical order is somewhere between fourth order and eighth order. Another method to design explicit derivative operators is by spectral matching of the response in the wavenumber domain (Holberg, 1987). This approach presents an improvement over the finite-difference method in the ability to propagate correctly short-wavelength components; however, the approach suffers from the same drawback of finite differences in that long-derivative operators fail to bring significant improvement in accuracy.

An alternative approach for spatial derivative calculation is to use implicit or recursive derivative operators that are based on a Padé approximation (Lele, 1992; Nagarajan et al., 2003; Zhou et al., 2008). The idea behind this approach is that rational expansions often converge faster than power series expansions, and, indeed, for a specified accuracy, this approach is more efficient than explicit finite differences; however, as with ordinary difference approximations, the

Manuscript received by the Editor 19 June 2009; revised manuscript received 4 December 2009; published online 20 October 2010.

¹Tel-Aviv University, Department of Geophysics, Tel-Aviv, Israel, and Paradigm Shenkar 9, Herzliya, Israel. E-mail: dan.kosloff@pdgm.com.

²Federal University of Bahia, Center for Research in Geophysics and Geology, Rua Barão de Geremoabo, Salvador, Bahia, Brazil. E-mail: reynam@cpgg.ufba.br.

³Tel-Aviv University, Computer Science, Academic College Tel-Aviv Yaffo, Tel-Aviv, Israel. E-mail: hillel@mta.ac.il.

© 2010 Society of Exploration Geophysicists. All rights reserved.

method is very accurate for the longer wavelengths but less accurate for the shorter wavelengths.

This study uses the concepts of Holberg (1987) for the design of explicit derivative operators for generating recursive derivative operators. The basic concept was first presented by Kosloff et al. (2008). The implicit filter coefficients are calculated by an L_∞ spectral fit in the wavenumber domain. This yields uniform accuracy within the range of wavenumbers that are used for the coefficient design. The derivative operators are designed by a Remes (1934a, b, c) exchange procedure (McClellan and Parks, 1972; Soubaras, 1996). This approach allows use of any number of terms in the numerator and in the denominator of the derivative operator, as opposed to the Padé approximation operators, in which only two terms are in the denominator. The application of these operators requires the solution of tridiagonal linear equation systems that can be carried out efficiently.

We describe the design of spatial derivative operators and compare their accuracy with the accuracy of explicit derivative operators. We then present a numerical example that compares simulations that have recursive operators with fourth-order finite-difference simulations and pseudospectral numerical simulations for the 2D constant density acoustic wave equation. The approach is then applied to the solution of the equations of 2D dynamic elasticity and tested against the analytical solution to Lamb's problem.

RECURSIVE SECOND-DERIVATIVE OPERATORS

Given a function $f(x)$, we denote its sampled values by $f[j] = f(x = jdx)$. The recursive second-derivative approximation can be written as

$$\frac{d^2f}{dx^2}[j] = \frac{a_0 + a_1\Delta_1 + a_2\Delta_2 + \dots + a_N\Delta_N}{1 + b_1\Delta_1 + b_2\Delta_2 + \dots + b_M\Delta_M} f[j], \quad (1)$$

where $\Delta_k f[j] = f[j + k] + f[j - k]$.

We consider operators for which $M \leq N$. In this case, equation 1 can be recast in an equivalent form:

$$\frac{d^2f}{dx^2}[j] = \left(c_0 + \dots + c_{N-M}\Delta_{N-M} + \frac{d_0}{1 + \beta_0\Delta_1} + \dots + \frac{d_{M-1}}{1 + \beta_{M-1}\Delta_1} \right) f[j]. \quad (2)$$

Equation 2 is more convenient for calculations, whereas equation 1 is more suitable for the design of the coefficients. The first terms in equation 2, $c_0 + \dots + c_{N-M}\Delta_{N-M}$, form an explicit operator. Each of the implicit terms $[dj/(1 + \beta_j\Delta_1)]f(j)$ forms a tridiagonal equation system. In terms of cost, each explicit term in equation 2 requires one multiplication, whereas each implicit term requires two multiplications (Zhou et al., 2008). The calculation of the coefficients c_0, c_1, \dots, c_{N-M} and $\beta_0, \dots, \beta_{M-1}$ from the coefficients in equation 1 is explained in Appendix A.

OPERATOR DESIGN

The coefficients a_1 and b_1 in equation 1 are calculated by an L_∞ norm fit in the spectral domain (McClellan and Parks, 1972; Soubaras, 1996). A substitution of $f[j] = e^{ikx} = jdx$ yields the fitting equation

$$a_0 + \sum_{j=1}^N 2a_j \cos(jkdx) + \sum_{j=1}^M 2b_j k^2 \cos(jkdx) = -k^2 \quad (3)$$

In the Remes (1934a, b, c) algorithm, the fitting equation is applied to $N + M + 2$ value of k , where an error term of alternating sign is added to each equation. The resulting $(N + M + 2) \times (N + M + 2)$ system of linear equations writes

$$a_0 + \sum_{j=1}^N 2a_j \cos(jk_L dx) + \sum_{j=1}^M 2b_j k_L^2 \cos(jk_L dx) + (-1)^L e = -k_L^2, \quad L = 1, \dots, N + M + 2. \quad (4)$$

The unknowns are $a_0, a_1, \dots, a_N, b_1, \dots, b_M$ and the error e . The $N + 2$ wavenumber components k_L are within the range $0 \leq k_L < k_{max}$, where k_{max} is specified by the user. The value of k_{max} should be set to give the best compromise between a small value of the error e and the largest wavenumber component that can be propagated with little numerical dispersion. The system in equation 4 is solved iteratively, whereby each time the $N + M + 2$ values of k_L are selected at the locations of the extreme of the error,

$$E(k) = a_0 + \sum_{j=1}^N 2a_j \cos(jkdx) + \sum_{j=1}^M 2b_j k^2 \cos(kjdx) + k^2$$

In this application, this procedure converges in a small number of iterations.

STAGGERED RECURSIVE FIRST-DERIVATIVE OPERATORS

Given a sampled function $f[j] = f(x = jdx), j = 0, \dots, Nx - 1$ the staggered first-derivative operator can be written as

$$\frac{df}{dx} \left[j + \frac{1}{2} \right] = \frac{a_0 \nabla_0 + a_1 \nabla_1 + a_2 \nabla_2 + \dots + a_N \nabla_N}{1 + b_1 \Delta_1 + b_2 \Delta_2 + \dots + b_M \Delta_M} f[j], \quad (5)$$

where $\Delta_k f[j + \frac{1}{2}] = f[j + k + 1] + f[j - k]$ and $\nabla_k f[j + \frac{1}{2}] = f[j + k + 1] - f[j - k], k = 0, 1, \dots$. This form of the operator maintains the required oddness of the first derivative.

The design of the coefficients a_i and b_i follows the same steps as in the design of the second-derivative operator in the previous section. The equations of the L_∞ fit are given by

$$\sum_{j=0}^N 2a_j \sin\left(\frac{k_L(2j+1)dx}{2}\right) + \sum_{j=1}^M 2b_j k_L \cos\left(\frac{k_L(2j+1)dx}{2}\right) + (-1)^L e = k_L, \quad L = 1, \dots, N + M + 2.$$

ACCURACY OF THE DERIVATIVE OPERATORS

We consider the application of the second-derivative operator to the function $f[j] = e^{ikjdx}$ for different k values and denote the output as $-k^2 f[j]$. Assuming that there are no errors in the time integration (through use of very small time steps or use of a high-accuracy time-integration scheme), the normalized numerical phase velocity is given by $c_f = k/\hat{k}$. Figure 1 plots the normalized phase velocity against wavenumber for different operators. In Figure 1, the curve marked fd-4 represents the fourth-order finite-differences operator, whereas 3-1, for example, denotes an operator obtained from equation 1 with $N = 3$ and $M = 1$, respectively. Figure 1 also shows the dispersion curve for the sixth-order Padé operator, the coefficients of which were taken from Liu and Sen (2009; Table 1). In the ideal case, the operator would yield a normalized phase velocity of 1 for all wavenumber components. In the design of the operators, the maximum wavenumber k_{max} was adjusted such that the maximum normalized phase-velocity error in the range $0 \leq k_i \leq k_{max}$ should be $< 0.5\%$.

Figure 1 shows that the inclusion of a rational term improved the accuracy of the derivative operator. In particular, the 3-1 operator produces a very good response. The 3-0 operator also has a better response than the fourth-order finite-difference operator, which contains the same number of coefficients.

Figure 2 compares the dispersion curves for the 3-1 operator, the sixth-order Padé operator (the coefficients of which were taken from Liu and Sen [2009; Table 1]), and the 5-0 operator. These operators require approximately the same amount of computational effort. Figure 2 shows that the implicit 3-1 operator is better than the explicit 5-0 operator and also better than the Padé operator, which has an identical structure. The improvement over the Padé operator is similar to the improvement that was reported by Holberg (1987) for explicit derivative operators.

Table 1 lists the coefficients in equation 1 which were calculated for different operators with $dx = 1$. In actual applications, the a_i coefficients need to be divided by dx^2 .

With regard to numerical stability, the numerical response of the recursive derivative operators is very close to the response of the pseudospectral method. Because the stability limit depends on the value of \hat{k}_{max} , the two methods have a very similar limit. In practice, to avoid numerical dispersion, one selects time-step sizes that are considerably smaller than the stability limit (Kosloff and Baysal, 1982).

NUMERICAL SOLUTION FOR ACOUSTIC AND ELASTIC

Wave propagation

For 2D acoustic wave propagation, the constant density wave equation is solved. The equation is given by

$$\frac{\partial^2 P}{\partial x^2} + \frac{\partial^2 P}{\partial y^2} = \frac{1}{c^2} \frac{\partial^2 P}{\partial t^2} + f, \tag{6}$$

where $P(x,y,t)$ denotes the pressure field, $c(x,y)$ is the acoustic velocity, and $f(x,y,t)$ is the source term. The spatial derivatives in equation 6 are calculated by using the recursive second-derivative operator. The solution is propagated in time by second-order time stepping. For avoidance of unwanted grid boundary reflections, absorbing regions were added along the boundaries (Kosloff and Kosloff, 1986).

For the equations of isotropic dynamic elasticity, the velocity-stress system is propagated, e.g., Carcione (2007), Operto et al. (2007), Kosloff and Carcione (2010). The system writes

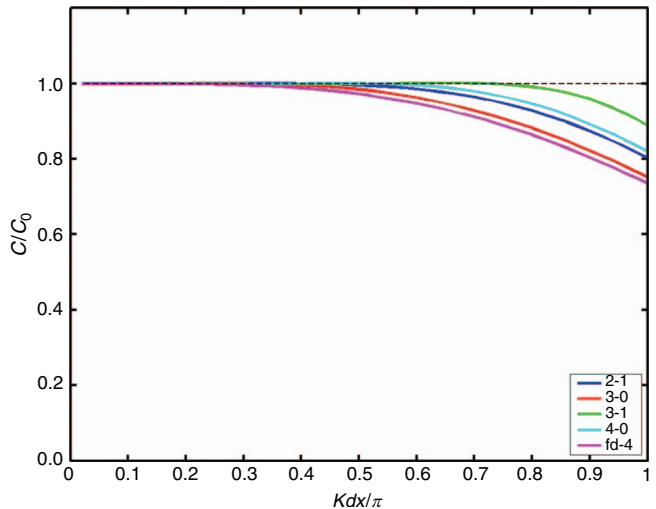


Figure 1. Normalized phase velocity versus normalized wavenumber Kdx/π for different second-derivative operators.

Table 1. Weights for different derivative operators.

	a_0	a_1	a_2	a_3	a_4	b_1
fd-2	-2	1	—	—	—	—
fd-4	$-\frac{5}{2}$	$\frac{4}{3}$	$-\frac{1}{12}$	—	—	—
fd-6	-2.722	1.5	-0.15	0.0111	—	—
3-0	-2.653	1.439	-0.1123	—	—	—
4-0	-2.928	1.663	-0.2262	0.0276	—	—
5-0	-3.070	1.789	-0.3129	0.0697	-0.0106	—
2-1	-2.470	1.235	—	—	—	0.1228
3-1	-2.090	0.8628	0.1823	—	—	0.2894

$$\frac{d}{dt} \begin{pmatrix} v_x \\ v_y \\ \sigma_{xx} \\ \sigma_{yy} \\ \sigma_{xy} \end{pmatrix} = \begin{pmatrix} -\gamma & 0 & \frac{1}{\rho} \frac{\partial}{\partial x} & 0 & \frac{1}{\rho} \frac{\partial}{\partial y} \\ 0 & -\gamma & 0 & \frac{1}{\rho} \frac{\partial}{\partial y} & \frac{1}{\rho} \frac{\partial}{\partial x} \\ (\lambda + 2\mu) \frac{\partial}{\partial x} & \lambda \frac{\partial}{\partial y} & -\gamma & 0 & 0 \\ \lambda \frac{\partial}{\partial x} & (\lambda + 2\mu) \frac{\partial}{\partial y} & 0 & -\gamma & 0 \\ \mu \frac{\partial}{\partial y} & \mu \frac{\partial}{\partial x} & 0 & 0 & -\gamma \end{pmatrix} \times \begin{pmatrix} v_x \\ v_y \\ \sigma_{xx} \\ \sigma_{yy} \\ \sigma_{xy} \end{pmatrix} + \begin{pmatrix} \frac{1}{\rho} f_x \\ \frac{1}{\rho} f_y \\ 0 \\ 0 \\ 0 \end{pmatrix}. \quad (7)$$

$v_x(x,y,t)$ and $v_y(x,y,t)$ denote the particle velocity in the x and y directions, respectively; $\sigma_{xx}(x,y,t)$, $\sigma_{yy}(x,y,t)$, and $\sigma_{xy}(x,y,t)$ are the stress components; $\lambda(x,y)$ and $\mu(x,y)$ are the shear modulus and the rigidity, respectively; $\rho(x,y)$ is the density; $f_x(x,y,t)$ and $f_y(x,y,t)$ are the body forces; and $\gamma(x,y)$ is an absorbing factor that differs from zero only along the boundaries of the numerical grid (Kosloff and Kosloff, 1986). The variables are located on a staggered grid in the following manner (Kosloff and Carcione, 2010):

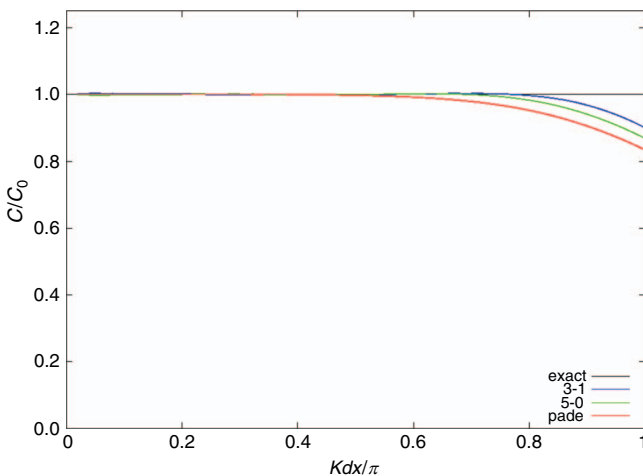


Figure 2. Normalized phase velocity versus normalized wavenumber Kdx/π for different second-derivative operators.

$$(i,j)\sigma_{xx}, \sigma_{yy}, \lambda, \lambda + 2\mu,$$

$$\left(i + \frac{1}{2}, j\right)v_x, f_x, \rho,$$

$$\left(i, j + \frac{1}{2}\right)v_y, f_y, \rho,$$

and

$$\left(i + \frac{1}{2}, j + \frac{1}{2}\right)\sigma_{xy}, \mu.$$

Material properties at half grid points are computed by averaging the values defined at regular points (Kosloff and Carcione, 2010).

The spatial derivatives in equation 7 are calculated by the recursive first-derivative operator. For the first and last nodes, the derivatives are calculated by second-order central differencing. The propagation of the solution in time is carried out by a fourth-order Runge-Kutta algorithm (Carcione, 2007).

The boundary conditions that were applied included rigid boundary conditions along the sides and bottom of the numerical mesh and a free surface boundary condition on the top. PML (perfectly matched layer) absorbing regions were applied along the sides and bottom of the mesh. The free surface boundary condition was imposed by the image method by setting

$$\sigma_{xy}\left(i + \frac{1}{2}, -\frac{1}{2}, ndt\right) = -\sigma_{xy}\left(i + \frac{1}{2}, \frac{1}{2}, ndt\right),$$

and

$$v_y\left(i, -\frac{1}{2}, ndt\right) = v_y\left(i, \frac{1}{2}, ndt\right)$$

$$+ dy \frac{\lambda(i,0)}{\lambda(i,0) + 2\mu(i,0)} \frac{\partial v_x}{\partial x}(i,0) \quad (8)$$

(Operto et al., 2007), where dy is the vertical grid spacing. The second condition in equation 8 combined with the calculation of the vertical derivative of v_y in the first row of nodes by second-order differencing ensures that $\sigma_{yy} = 0$ at the surface and that σ_{xx} there is calculated in a consistent manner.

To improve the calculation of surface waves in the vicinity of the free surface, we used a variable mesh in which the grid spacing near the surface is reduced (Kosloff and Carcione, 2010). The mapping function is given by

$$y(\xi) = dy \times \left(\frac{1 + \alpha}{2} \xi - \frac{1 - \alpha}{2} \frac{\xi_0}{\pi} \sin \frac{\pi \xi}{\xi_0} \right), \quad (9)$$

where ξ_0 is the number of grid points in the stretch region; ξ is the grid number in the y direction; and α is a stretch factor, e.g., the grid size on the surface is $\approx \alpha dy$. The derivatives with respect to y are calculated by a chain rule,

$$\frac{\partial f}{\partial y} = \frac{\partial f}{\partial \xi} \times \frac{d\xi}{dy},$$

where,

$$\frac{dy}{d\xi} = dy \left(\frac{1-\alpha}{2} \left[1 - \cos \frac{\pi\xi}{\xi_0} \right] + \alpha \right).$$

Typical values for the parameters are $\xi_0 = 30$ and $\alpha = 0.2$

Examples

Migration of a synthetic data set

The numerical derivative operators were tested in a 2D example of zero-offset reverse-time migration with the constant density acoustic wave equation. The subsurface model consisted of a single reflector with two segments dipping in opposite directions and one horizontal segment (Figure 3). The model has a constant velocity of 4500 m/s. The maximum frequency in this example was 80 Hz, the horizontal and vertical grid spacing was 27 m, and the time step was 2 ms. The input time section was obtained by numerical modeling using the program SusyInv from the Seismic Unix-SU Package. Figure 4a-d, respectively, show migrated images that were obtained with the fourth-order finite-difference method, the 2-1 operator method, the 3-1 operator method, and the pseudospectral method. The choice of the maximum frequency depends on the dispersion condition. Considering $G = 5$, where G is the number of points per wavelength, the highest frequency allowed by the fourth-order finite-difference scheme to avoid dispersion should be <16.7 Hz. As Figure 4 shows, the numerical dispersion is most prominent in Figure 4a of the fourth-order finite-difference method. Figure 4b of the 2-1 recursive method is somewhat improved, whereas the improvement in Figure 4c of the 3-1 recursive method is very obvious. In fact, the result in Figure 4c is almost as good as the result of the pseudospectral method in Figure 4d.

Lamb's problem

Numerical and analytic solutions are compared for the problem of a vertical point source embedded in a uniform 2D isotropic elastic half-space. The analytical solution is obtained by the method of Cagniard-De Hoop (Berg et al., 1994).

The medium parameters were $v_p = 2000$ m/s, $v_s = 1155$ m/s, and $\rho = 2000$ kg/m³. The point source was located 2 m beneath the free surface and had a Ricker wavelet time history with a central frequency of 10 Hz. It was applied as a force term on a single node. The numerical solution used a grid that contained 440 points in the horizontal direction and 220 points in the vertical direction. The horizontal grid spacing was 10 m. The vertical grid spacing was 10 m away from the free surface. Grid compression was used in the upper part of the grid with values of $\xi_0 = 50$ and $\alpha = 0.1$ in equation 9. The calculations were carried out to $t = 2$ s.

Figures 5 and 6, respectively, show snapshots of the horizontal and vertical particle velocities at $t = 0.8$ s. In the figures, the P-wave and the S-

wave as well as the PS converted head wave. The Rayleigh wave is most prominent in the vicinity of the free surface, and it slightly lags behind the S-wave, as predicted (for the selected parameters $V_R \approx 0.92V_S$).

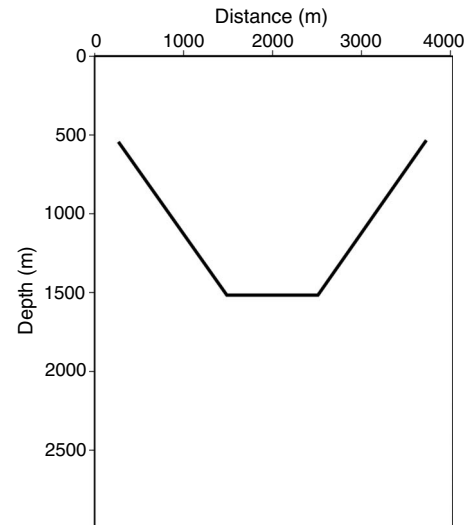


Figure 3. Depth model: Constant velocity.

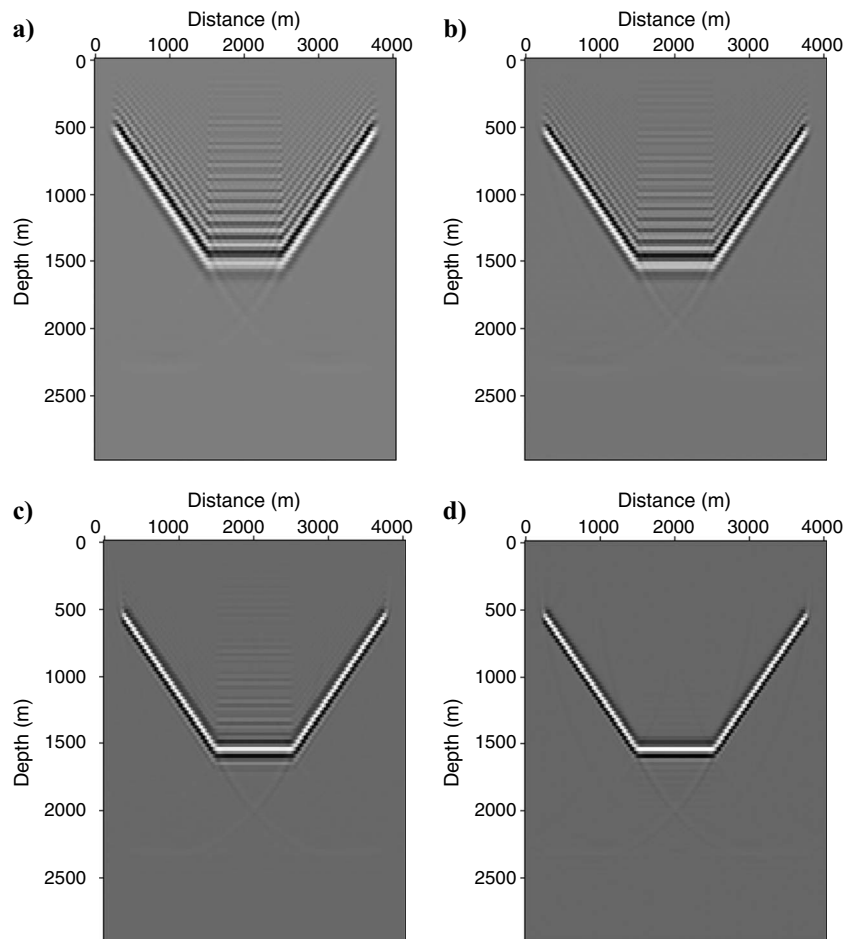


Figure 4. Reverse-time migration results. (a) Fourth-order finite-difference operator (4-0); (b) implicit operator (2-1); (c) implicit operator (3-1), and (d) pseudospectral method.

The first comparison between numerical and analytic solutions is for a shallow receiver located at a large distance from the source. In this range, the solution is dominated by the Rayleigh wave, which poses a challenge to numerical simulations. Figures 7 and 8, respectively, compare numerical and analytical solutions for the horizontal particle velocity and the vertical particle velocity for a receiver located 2 m beneath the surface at a horizontal distance of 1400 m from the source. As the figures show, the comparison is quite satisfactory for both horizontal and vertical components.

Figures 9 and 10 compare numerical and analytic solutions for

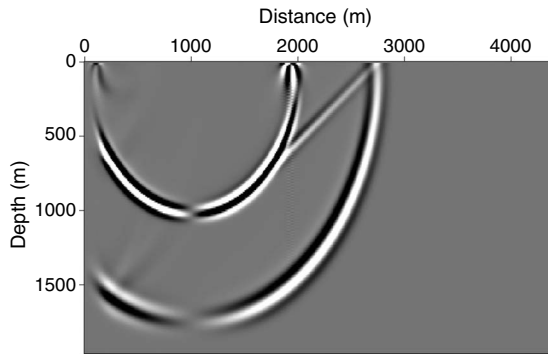


Figure 5. Elastic modeling constant velocity case: Horizontal velocity particle snapshot at $t = 0.8$ s.

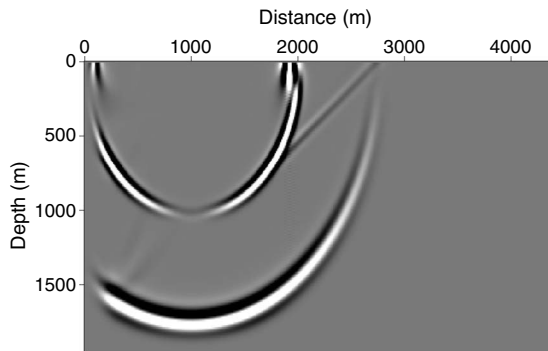


Figure 6. Elastic modeling constant velocity case: Vertical velocity particle snapshot at $t = 0.8$ s.

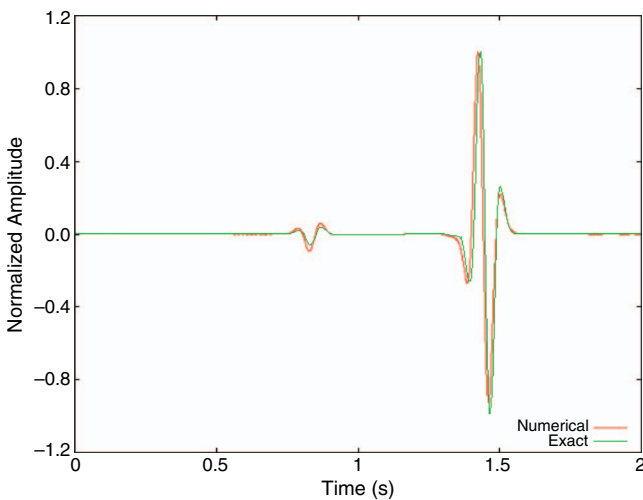


Figure 7. Comparison between numerical and analytical solution for the horizontal velocity particle located at $x = 1400$ m and $z = 2$ m from the source.

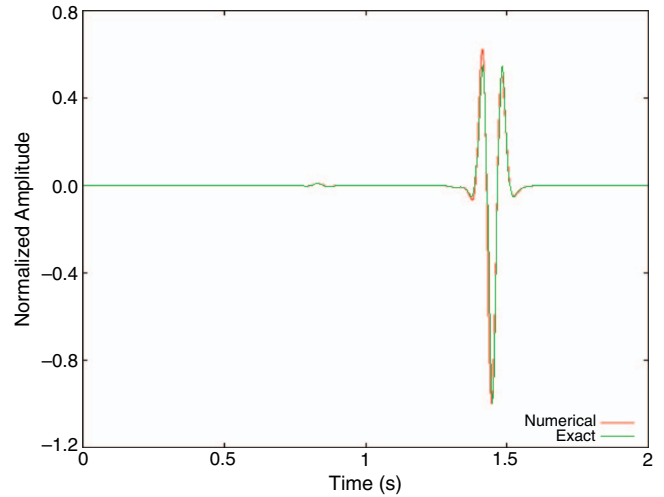


Figure 8. Comparison between numerical and analytical solution for the vertical velocity particle located at $x = 1400$ m and $z = 2$ m from the source,

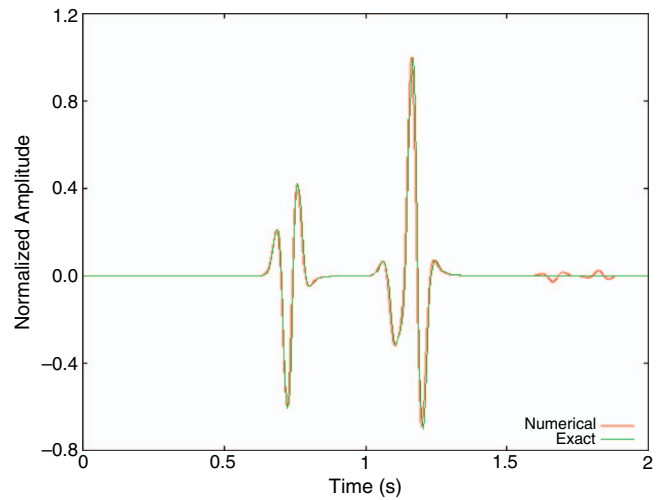


Figure 9. Comparison between numerical and analytical solution for the horizontal velocity particle located at $x = 1000$ m and $z = 675$ m from the source.

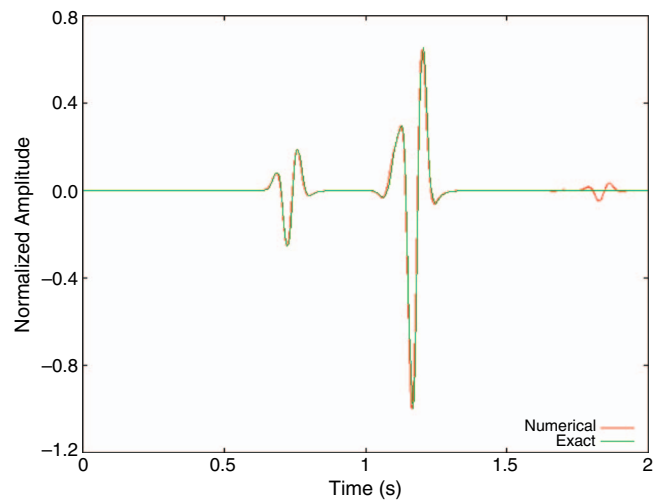


Figure 10. Comparison between numerical and analytical solution for the vertical velocity particle located at $x = 1000$ m and $z = 675$ m from the source.

horizontal and vertical particle velocities at a receiver located at a horizontal distance of 1000 m from the source at a depth of 650 m. Again, the comparisons between the numerical and analytical solutions are very good.

CONCLUSIONS

We have presented a new scheme for calculating first and second spatial derivatives on a grid that is based on recursive operators. The method is based on applying recursive operators in each of the spatial coordinates. The operators were designed by a fit of the response in the wavenumber domain. It was shown that these operators enable extension of numerical solutions to shorter wavelengths while saving in computer time. It seems that the addition of a single rational term in the derivative operator significantly increases its effectiveness.

The application of the recursive derivative operators involves solution of tridiagonal linear equation systems. Such systems can be solved with approximately $2N$ mathematical operations, where N is the number of sample points. This number is approximately twice the number of operations that are required for calculating derivatives with explicit operators. The method of this study can also be applied to 3D, for which the recursive operators are applied separately in the three coordinate directions.

ACKNOWLEDGMENTS

We thank three anonymous reviewers, whose comments helped significantly to improve the manuscript.

APPENDIX A

DERIVATION OF THE COEFFICIENTS IN EQUATION 2

Given the coefficients $a_i, i = 0, \dots, N$ and $b_i, i = 1, \dots, M$ in equation 1, the coefficients in equation 2 can be calculated from them analytically; however, in this study, we chose to derive them by a numerical procedure that is easy to implement.

First, equation 1 is recast in an alternative form:

$$\frac{a_0 + a_1 \Delta_1 + a_2 \Delta_2 + \dots + a_N \Delta_N}{1 + b_1 \Delta_1 + b_2 \Delta_2 + \dots + b_M \Delta_M} f[j] = \frac{a'_0 + a'_1 \Delta_1 + a'_2 \Delta_1^2 + \dots + a'_N \Delta_1^N}{b'_0 + b'_1 \Delta_1 + b'_2 \Delta_1^2 + \dots + b'_M \Delta_1^M} f[j]. \quad (\text{A-1})$$

The coefficients b'_i on the righthand side of equation A-1 can be related to the coefficients b_i on the lefthand side by choosing $f[j] = e^{ikjdx}$ and equating the denominators on both sides of equation A-1. The resulting equation writes

$$1 + 2b_1 \cos kdx + 2b_2 \cos 2kdx + \dots + 2 \cos Mkdx = b'_0 + 2b'_1 \cos kdx + 4b'_2 \cos^2 kdx + \dots + 2^M b'_M \cos^M kdx. \quad (\text{A-2})$$

By selecting M values of k , which yield different values of $\cos kdx$, i.e., they should not be equal to 2π , we obtain a set of M linear equations in M unknowns for the b'_i coefficients.

The β_i coefficients in equation 2 are then given by $\beta_i = -1/\lambda_i$, where $\lambda_i, i = 1, \dots, M$ are the roots of the polynomial

$$P(x) = b'_0 + b'_1 x + b'_2 x^2 + \dots + b'_M x^M.$$

Finally, $c_i = 0, \dots, N - M$ and $d_i = 0, \dots, M - 1$ in equation 2 are calculated by solving the set of $N + 1$ linear equation in $N + 1$ unknowns:

$$c_0 + 2c_1 \cos k_\alpha dx + \dots + 2c_{N-M} \cos(N-M)k_\alpha dx + \frac{d_0}{1 + 2\beta_0 \cos k_\alpha dx} + \dots + \frac{d_{M-1}}{1 + 2\beta_{M-1} \cos k_\alpha dx} = \frac{a_0 + 2a_1 \cos k_\alpha dx + \dots + 2a_N \cos Nk_\alpha dx}{1 + 2b_1 \cos k_\alpha dx + \dots + 2b_M \cos Mk_\alpha dx},$$

where $\alpha = 0, \dots, N$

for different values of $\cos k_\alpha dx$. The righthand side of this equation is known.

REFERENCES

- Berg, P., I. Flemming, P. Nielsen, and O. Skovgaard, 1994, Analytical reference solutions, in K. Helbig, ed., Modeling the earth for oil exploration: Pergamon Press, 421–427.
- Carcione, J. M., 2007, Wave fields in real media: Theory and numerical simulation of wave propagation in anisotropic, anelastic, porous and electromagnetic media 2nd edition, revised and extended: Elsevier Science.
- Dablain, M. A., 1986, The application of high-order differencing to the scalar wave equation: Geophysics, **51**, 54–66, doi: 10.1190/1.1442040.
- Holberg, O., 1987, Computational aspect of the choice of operator and sampling interval for numerical differentiation in large scale simulation of wave phenomena: Geophysical Prospecting, **35**, no. 6, 629–655, doi: 10.1111/j.1365-2478.1987.tb00841.x.
- Kosloff, D., and E. Baysal, 1982, Forward modeling by the fourier method: Geophysics, **47**, 1402–1412, doi: 10.1190/1.1441288.
- Kosloff, D., and J. M. Carcione, 2010, 2D simulation of Rayleigh waves with staggered sine/cosine transforms and variable grid spacing: Geophysics, **75**, no. 4, T133–T140.
- Kosloff, D., A. Q. Filho, E. Tessmer, and A. Behle, 1989, Numerical solution of the acoustic and elastic wave equations by a new rapid expansion method (REM): Geophysical Prospecting, **37**, no. 4, 383–394, doi: 10.1111/j.1365-2478.1989.tb02212.x.
- Kosloff, D., and R. Kosloff, 1986, Absorbing boundaries for wave propagation problems: Journal of Computational Physics, **63**, no. 2, 363–376, doi: 10.1016/0021-9991(86)90199-3.
- Kosloff, D., R. C. Pestana, and H. Tal-Ezer, 2008, Numerical solution of the constant density acoustic wave equation by implicit spatial derivative operators: 78th Annual International Meeting, SEG, Expanded Abstracts, 2057–2061.
- Lele, S. K., 1992, Compact finite difference schemes with spectral-like resolution: Journal of Computational Physics, **103**, no. 1, 16–42, doi: 10.1016/0021-9991(92)90324-R.
- Liu, Y., and M. K. Sen, 2009, A practical implicit finite-difference method: Examples from seismic modelling: Journal of Geophysics and Engineering, **6**, no. 3, 231–249, doi: 10.1088/1742-2132/6/3/003.
- Liu, F., G. Zhang, S. Morton, and J. P. Leveille, 2009, An optimized wave equation for seismic modeling and reverse time migration: Geophysics, **74**, no. 6, WCA153–WCA158, doi: 10.1190/1.3223678.
- McClellan, J. H., and T. W. Parks, 1972, Equiripple approximation of fan filters: Geophysics, **37**, 573–583, doi: 10.1190/1.1440284.
- Nagarajan, S., S. K. Lele, and J. Ferziger, 2003, A robust high-order compact method for large eddy simulation: Journal of Computational Physics, **191**, no. 2, 392–419, doi: 10.1016/S0021-9991(03)00322-X.
- Operto, S., R. Brossier, and J. Virieux, 2007, 2D P-SV finite difference time domain modelling of elastic wave propagation: Technical report 7-SEISCOPE project.
- Remes, E. Y., 1934a, Sur la détermination des polynômes d'approximation de degré donnée: Communications of the Kharkov Mathematical Society, **10**, 41.
- , 1934b, Sur le calcul effectif des polynômes d'approximation des tschebyscheff: Comptes Rendus de l'Académie des sciences, **199**, 337.
- , 1934c, Sur un procédé convergent d'approximations successives pour déterminer les polynômes d'approximation: Comptes Rendus de l'Académie des sciences, **198**, 2063.
- Soubaras, R., 1996, Explicit 3d migration using equiripple polynomial ex-

pansion and laplace synthesis: *Geophysics*, **61**, 1386–1393, doi: 10.1190/1.1444062.

Stoffa, P. L., and R. C. Pestana, 2009, Numerical solution of the acoustic wave equation by the rapid expansion method (REM) — A one step approach: 79th Annual International Meeting, SEG Expanded Abstracts,

2672–2675.

Zhou, H., Q. Liao, and F. Ortigosa, 2008, Construction and analysis of an optimized compact finite difference scheme for RTM: Presented at the 70th Annual Meeting of the European Association of Geoscientists and Engineers.